ISSN 2517-7516, Membranes and Membrane Technologies, 2021, Vol. 3, No. 6, pp. 377–388. © Pleiades Publishing, Ltd., 2021.
Russian Text © The Author(s), 2021, published in Membrany i Membrannye Tekhnologii, 2021, Vol. 3, No. 6, pp. 422–434.

Perovskites Based on $SrCo_{0.8}Fe_{0.2}O_{3-\delta}$ (SCF) and $Ba_{0.5}Sr_{0.5}Co_{0.8}Fe_{0.2}O_{3-\delta}$ (BSCF) Oxides and Their Application as Membrane Materials and Electrodes for Solid Oxide Fuel Cells

E. V. Shubnikova[a, *] and A. P. Nemudry[a, b]

[a] *Institute of Solid State Chemistry and Mechanochemistry, Siberian Branch, Russian Academy of Sciences, Novosibirsk, 630128 Russia*

[b] *Novosibirsk State University, Novosibirsk, 630090 Russia*

**e-mail: artimonovalena@yandex.ru*

Received July 12, 2021; revised August 5, 2021; accepted August 11, 2021

Abstract—This review describes perovskites based on $SrCo_{0.8}Fe_{0.2}O_{3-\delta}$ (SCF) and $Ba_{0.5}Sr_{0.5}Co_{0.8}Fe_{0.2}O_{3-\delta}$ (BSCF) oxides, which are thought of as promising materials for catalytic membrane reactors and solid oxide fuel cells (SOFCs). Data on the oxygen permeability of disk-shaped and microtubular membranes based on SCF and BSCF oxides are discussed; special attention is paid to methods used to increase the oxygen permeability of membrane materials and improve their phase/structural stability. The review describes the electrochemical characteristics of promising cathode materials based on SCF and BSCF perovskites and provides a summary of the latest developments.

Keywords: perovskites, mixed ionic–electronic conductivity oxides, oxygen-permeable membranes, solid oxide fuel cells

DOI: 10.1134/S251775162106007X

INTRODUCTION

Complex oxides with an ABO_3 perovskite structure exhibit a set of unique physicochemical properties; therefore, they have been attracting the attention of researchers for many years. High-temperature superconductivity [1, 2], magnetoresistance [3], ferromagnetism, ferroelectricity [4], catalytic activity [5, 6], superionic conductivity [7, 8], and other properties make it possible to use perovskites in various innovation areas. Perovskites $ABO_{3-\delta}$ with transition metal cations (B = Mn, Fe, Co, Ni, Cu), which are capable of changing the oxidation state (change is compensated by a change in oxygen stoichiometry), exhibit mixed oxygen–electronic conductivity (MOEC). Owing to a change in the oxygen stoichiometry of MOEC perovskites upon interaction with a gaseous phase ($ABO_{3-\delta} + 1/2\delta O_2 \leftrightarrow ABO_3$) and the fact that they exhibit high ionic (oxygen) and electronic conductivity, MOEC perovskites can be used as oxygen-reversible electrode materials in solid oxide fuel cells (SOFCs), oxygen-permeable membranes and sorbents exhibiting 100% oxygen selectivity, partial pressure sensors, etc. The combination of oxygen separation and partial oxidation of hydrocarbons in catalytic membrane reactors (CMRs) using oxygen-permeable membranes based on MOEC perovskites leads to a significant decrease in the synthesis gas production cost [9, 10]. According to data first published by Teraoka and Shao [11, 14], $SrCo_{0.8}Fe_{0.2}O_{3-\delta}$ (SCF) and $Ba_{0.5}Sr_{0.5}Co_{0.8}Fe_{0.2}O_{3-\delta}$ (BSCF) perovskites have the best transport characteristics of all MOEC perovskites and are of significant interest for designing materials used in innovative technologies. However, the use of materials based on these oxides is limited due to the occurrence of phase transitions (perovskite–brownmillerite for SCF, cubic–hexagonal perovskite for BSCF) and the low chemical stability in a CO_2 atmosphere. These problems are generally solved using the isomorphic substitution of cations in the A and B sublattices of the oxide. This manuscript is a review of studies on the doping of SCF/BSCF oxides aimed at increasing their phase and chemical stability and improving the oxygen permeability and electrochemical characteristics of membranes and electrodes based on these oxides.

MIXED OXYGEN–ELECTRONIC CONDUCTIVITY OXIDES AS MEMBRANE MATERIALS

Oxygen is thought of as one of the most commonly used gases in modern industrial processes. Despite the fact that oxygen is among the most abundant chemical elements on Earth, the production of pure oxygen

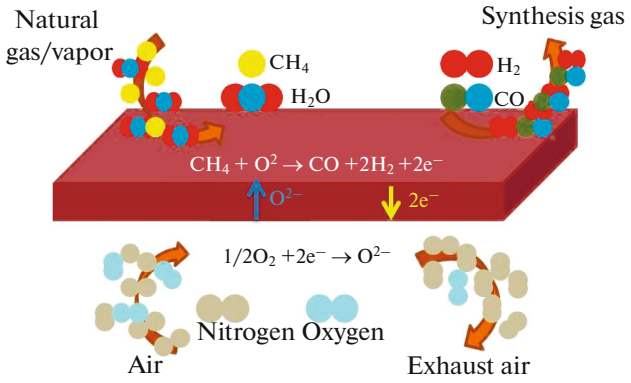

Fig. 1. Principle of operation of a selective oxygen-permeable membrane integrated into the process for the partial oxidation of hydrocarbons.

(e.g., the cryogenic distillation method) is an expensive and energy-intensive process [11].

Currently, the development of pure oxygen production technologies is thought of as a promising direction. The development and implementation of technologies for the deep processing of natural gas will make it possible to take a step toward the environmentally sustainable development of the country.

Recently, the gas to liquid (GTL) technology has developed quite intensively; it includes the stage of partial oxidation of methane:

$$CH_4 + O_2 = CO + H_2. \quad (1)$$

Synthesis gas is a precursor for the production of some important chemical compounds, such as ammonia and methanol; according to economic estimates, the world production of these compounds is 10^8 and 10^7 ton per year, respectively. Methanol acts as a reagent for the synthesis of a large chain of organic compounds and polymers [12]. However, fairly high capital expense and energy costs limit the use of the GTL technology. Recently, the world's leading gas companies have exhibited vigorous activities toward the development of an innovative method for producing synthesis gas ($CO + H_2$) in CMRs. In this method, the catalytic partial oxidation of methane occurs on the surface of a ceramic membrane exhibiting selective oxygen permeability (see Fig. 1). The use of air as an oxygen source makes it possible to significantly simplify the process unit and can lead to a 30% decrease in the cost of synthesis gas.

The general principles of operation of oxygen-permeable membranes are described in detail in a number of papers [13, 14, 62, 63].

It is well known that the commercial use of the GTL technology requires materials with the following characteristics: (i) high oxygen permeability, (ii) thermochemical and long-term stability, and (iii) low cost of materials.

Analysis of the published data shows that SCF and BSCF perovskite-like oxides exhibit the best oxygen fluxes and are promising materials in the field of designing membranes for CMRs [11, 14, 15].

DISK-SHAPED MEMBRANES BASED ON SCF AND BSCF

The development of oxygen-permeable membranes for CMRs requires studying the oxygen exchange processes in MOEC oxides (studying the reaction mechanisms, identifying possible methods and techniques to modify transport properties).

According to the published data, the SCF perovskite-like oxide exhibits a high oxygen permeability [11]. However, in a medium with a low partial pressure of oxygen, this compound is characterized by the ordering of oxygen vacancies and the formation of a brownmillerite structure, which leads to a decrease in oxygen fluxes and the degradation of the membrane under operating conditions. In addition, SCF-based compounds are chemically unstable in a CO_2 atmosphere, where the oxygen fluxes significantly decrease due to the formation of carbonates on the membrane surface [16, 17]. These problems limit the possibilities of using SCF oxides and, therefore, require a modification of their properties. The currently available methods for modifying the properties of SCF oxides are as follows: (i) the introduction of cations with a stable oxidation state into the A and B sites of the perovskite structure, (ii) a decrease in the membrane thickness, and (iii) the surface modification of the membrane via depositing catalytically active metals (Pt, Pd, Ag, etc.) and porous layers.

One of the most commonly used methods to increase oxygen fluxes is the isomorphic substitution of $Co^{3+/4+}$ cations in an SCF oxide by cations with a stable oxidation state [18–23]. Table 1 shows the oxygen permeability of doped SCF compounds. Typically, the B-site doping of an SCF oxide leads to a decrease in the oxygen permeability. For example, the introduction of Al^{3+}, Zr^{4+}, and Ti^{4+} cations can lead to a significant increase in the phase and chemical stability of the materials; however, the oxygen flux decreases with an increase in the dopant content in the oxide. The cited authors attribute these effects to the so-called "trap effect," which is the interaction of the dopant with mobile defects, i.e., charge carriers (oxygen vacancies) [17].

It is fairly well known that SCF-based oxides are unstable in a CO_2 atmosphere due to the formation of carbonates on the membrane surface. Over time, this factor leads to a significant decrease in the oxygen permeability of the membrane. The authors of [21] showed a decrease in the adverse effect of CO_2 on the oxygen permeability of SCF-based oxides. In that study, it was shown that, in a CO_2 atmosphere, the oxygen flux of a disk-shaped membrane based on

Table 1. Published data on the oxygen fluxes and activation energies for oxygen transport of disk-shaped membranes based on SCF and BSCF oxides

Composition	Conditions	L, mm	$J(O_2)$, mL/(min cm^2)	E_a, kJ/mol
$SrCo_{0.8}Fe_{0.2}O_{3-\delta}$ [11]	$T = 800°C$; $pO_{2.1} = 0.2$ atm	1	1.53	86
$Ba_{0.5}Sr_{0.5}Co_{0.8}Fe_{0.2}O_{3-\delta}$ [14]	$T = 900°C$; $pO_{2.1} = 0.2$ atm	1	1.94	42
$Ba_{0.5}Sr_{0.5}Co_{0.8}Fe_{0.2}O_{3-\delta}$ [42]	$T = 900°C$; $pO_{2.1} = 0.2$ atm	1	1.82	31–48
$Ba_{0.5}Sr_{0.5}Co_{0.8}Fe_{0.2}O_{3-\delta}$ [31]	$T = 900°C$; $pO_{2.1} = 0.2$ atm	1	1.72	–
$SrCo_{0.8}Fe_{0.1}Nb_{0.1}O_{3-\delta}$ [22]	$T = 900°C$; $pO_{2.1} = 0.2$ atm	1	2.12	–
$Sr(Co_{0.8}Fe_{0.2})_{0.98}Zr_{0.02}O_{3-\delta}$ [20]	$T = 900°C$; $pO_{2.1} = 0.2$ atm	1	1.71	–
$Sr(Co_{0.8}Fe_{0.2})_{0.9}Ta_{0.1}O_{3-\delta}$ [21]	$T = 900°C$; $pO_{2.1} = 0.2$ atm	1	1.16	–
$SrAl_2O_4$-SCF(3%) [19]	$T = 900°C$; $pO_{2.1} = 0.2$ atm	1	1.85	–
$Sr(Co_{0.8}Fe_{0.1})_{0.8}Ti_{0.2}O_{3-\delta}$ [23]	$T = 950°C$; $pO_{2.1} = 0.2$ atm	1	0.91	69.6 ± 10.1
$SrCo_{0.75}Fe_{0.1}Mo_{0.05}O_{3-\delta}$ [18]	$T = 900°C$; $pO_{2.1} = 0.2$ atm	1.5	1.18	55 ± 10
$Ba_{0.5}Sr_{0.5}(Co_{0.8}Fe_{0.2})_{0.98}Zn_{0.02}O_{3-\delta}$ [31]	$T = 900°C$; $pO_{2.1} = 0.2$ atm	1	1.98	–
$Ba_{0.5}Sr_{0.5}Co_{0.79}Fe_{0.2}Y_{0.01}O_{3-\delta}$ [32]	$T = 900°C$; $pO_{2.1} = 0.2$ atm.	1.2	1.70	–
$(Ba_{0.5}Sr_{0.5})(Co_{0.8}Fe_{0.2})_{0.97}Zr_{0.03}O_{3-\delta}$ [33]	$T = 900°C$; $pO_{2.1} = 0.2$ atm	1	1.64	34–64
$Ba_{0.5}Sr_{0.5}Co_{0.7}Fe_{0.2}Nb_{0.1}O_{3-\delta}$ [13]	$T = 900°C$; $pO_{2.1} = 0.2$ atm	1	1.95	50
$Ba_{0.5}Sr_{0.5}Co_{0.78}Fe_{0.2}W_{0.02}O_{3-\delta}$ [24]	$T = 900°C$; $pO_{2.1} = 0.2$ atm	1.6	1.80	65

$Sr(Co_{0.8}Fe_{0.2})_{0.9}Ta_{0.1}O_{3-\delta}$ (SCFTa) remained at a level of $J_{O_2} \sim 1.16$ mL/(min cm^2) for 100 h, unlike an SCF membrane, where the oxygen fluxes underwent significant degradation until their complete cessation.

Studies of the transport characteristics of oxides based on $SrTi_{1-x-y}Co_xFe_yO_{3-\delta}$ (STCF, $x + y \le 0.35$) are described in [22]. The cited authors showed that STCF disk-shaped membranes (content of $x + y = 0.25$) have oxygen fluxes at a level of $J_{O_2} \sim 0.12$ mL/(min cm^2), which remain stable at $T = 900°C$ for 140 h. However, studies of the thermochemical stability of STCF ($x + y \le 0.35$) oxides under synthesis gas production conditions showed the formation of additional phases of the Ruddlesden–Popper type, Co_3O_4, and $SrCO_3$, which significantly limits the use of these oxides as membranes for CMRs.

According to [24, 25], high oxygen fluxes for SCF oxides were achieved upon the substitution of the Sr^{2+} cation by La^{2+} and Ba^{2+} cations. At the same time, the BSCF oxide has the highest oxygen flux values of all known perovskites. It was shown [14, 15] that the oxygen permeability of disk-shaped BSCF membranes ($L = 1$ mm) was $J_{O_2} \sim 1.63$ mL/(min cm^2) at $T = 950°C$ (helium flow rate of $F_{He} = 80$ mL/min). According to the authors, the rate-limiting step of the oxygen transport process in the BSCF oxide is solid-phase diffusion. However, in an atmosphere with a high oxygen content at $T \le 850°C$, the BSCF oxide is characterized by the formation of a hexagonal structure with a low oxygen mobility. Microscopic studies showed that the hexagonal phase is localized along the grain boundaries, which is a barrier to oxygen transport [26, 27]. As a consequence, the oxygen fluxes of the BSCF oxide decrease over time: according to studies of long-term stability, at $T = 750°C$ in an air atmosphere, the oxygen flux of the BSCF oxide decreases twofold after 240 h [27]. It was shown [28] that the partial substitution of $Co^{3+/4+}/Fe^{3+}$ cations by yttrium cations in the BSCF structure can hinder phase transformations into a hexagonal phase. Ex situ diffraction studies of the $Ba_{0.5}Sr_{0.5}(Co_{0.8}Fe_{0.2})_{0.9}Y_{0.1}O_{3-\delta}$ (BSCF10Y) oxide after a long-term annealing at $T = 800°C$ for 44 days showed that the initial temperature of the formation of the hexagonal phase is shifted toward lower temperatures. The hexagonal phase is detected only after annealing at $T \le 760°C$, unlike the case of the BSCF oxide.

It is of interest that the use of membranes based on the BSCF oxide faces a problem of the formation of carbonates on the surface, which leads to a significant decrease in the oxygen permeability. It was shown [29] that the feeding of 15% CO_2 to a disk-shaped membrane based on BSCF leads to a considerable decrease—almost to zero values—in the oxygen fluxes. Other authors [30] showed that the adverse effect of CO_2 is reversible. Upon the removal of CO_2 from the reaction mixture, the oxygen fluxes return to their initial values. However, it was found that, under the conditions of the partial oxidation of methane, the perovskite phase undergoes decomposition to form Co_3O_4 and $BaCO_3$ oxides and an unidentified phase.

The oxygen permeability of disk-shaped membranes based on the BSCF oxide was described in [13,

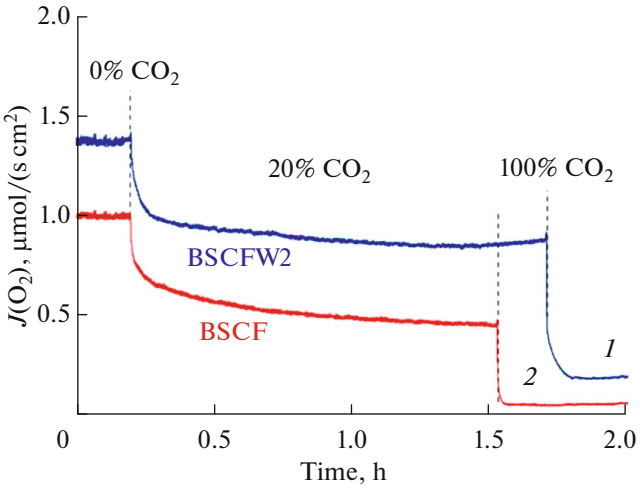

Fig. 2. Time dependence of oxygen flux of (*1*) BSCFW2 and (*2*) BSCF disk-shaped membranes as a function of CO_2 content.

24, 31–33]; the results are shown in Table 1. The effect of doping with Zn^{2+} cations on the oxygen permeability of disk-shaped membranes based on the BSCF oxide was studied in [31]. The results of the study showed that the introduction of Zn^{2+} into the structure of the BSCF oxide lead to a significant increase in the oxygen fluxes. Despite this fact, the problem of the formation of hexagonal phases has not been solved. According to the results of the study, an increase in the carrier gas flow rate leads to an increase in the oxygen permeability of $Ba_{0.5}Sr_{0.5}(Co_{0.8}Fe_{0.2})_{1-x}Zn_xO_{3-\delta}$ oxides. The cited authors assumed that the rate-limiting step of the oxygen transport process is the diffusion of oxygen ions through the membrane. However, according to our reckoning, these studies are insufficient to describe the oxygen permeation mechanism. To identify the rate-limiting steps of the oxygen transport process, it is necessary to conduct further studies, in particular, with membranes having different thicknesses.

An approach to modifying the properties of perovskite-like oxides has been developed at Institute of Solid State Chemistry and Mechanochemistry of the Siberian Branch of the Russian Academy of Sciences [34–36]; it consists in doping MOEC oxides with ferroactive highly charged cations B^{5+} (Nb, Ta) and B^{6+} (Mo, W). The strategy is based on the idea that perovskites are ferroics. Recent studies [24, 25, 37–43] have shown that the introduction of ferroactive highly charged cations into the structure of SCF/BSCF-based MOEC oxides can have a significant effect on the microstructure of the compounds, suppress undesirable phase transformations and, thereby, improve the transport properties of the materials. According to [24, 25, 43], doping of BSCF with highly charged cations W^{6+} and Mo^{6+} leads to an improvement of the stability of oxygen fluxes in a CO_2 atmosphere. The authors of [25] showed that, under exposure to an atmosphere containing 20% CO_2, oxygen fluxes decrease by a factor of 2.2 and 1.4 for BSCF and $Ba_{0.5}Sr_{0.5}Co_{0.78}Fe_{0.2}W_{0.02}O_{3-\delta}$ (BSCFW2) disk-shaped membranes, respectively (Fig. 2). However, after the decrease, the oxygen fluxes of the disk-shaped membrane based on the BSCFW2 oxide undergo stabilization, unlike the fluxes of BSCF.

SURFACE MODIFICATION OF MEMBRANES

In membranes of MOEC oxides with thickness L, the chemical potential gradient is the driving force of oxygen transport. If the membrane thickness is $L < L_c$ (L_c is the characteristic thickness), then the rate-limiting step of oxygen transport is reactions on the surface [9]. In this case, the rate of oxygen exchange on the surface and, thereby, the total oxygen flux can be increased by increasing the active surface area of the membrane via depositing porous layers or catalysts (e.g., Pt, Ag) on the surface [40]. In addition, the use of catalysts makes it possible to decrease the operating temperature of membranes/cathodes based on MOEC oxides, which is a key technological problem in their use.

It was shown [40] that the deposition of silver (Ag) on the surface from the permeate side of a $SrCo_{0.8-x}Fe_{0.2}Mo_xO_{3-\delta}$ membrane leads to an increase in the oxygen fluxes by a factor of 1.8, while the activation energy for the oxygen transport process does not change. The cited authors report that Ag effectively accepts electrons and delivers them to ions in the B-site of the perovskite structure (e.g., Fe^{4+}), rather than decreases the activation energy for the rate-limiting step of oxygen transport. That is, formally, an increase in the concentration of active sites on the membrane surface (preexponential factor) takes place.

The oxygen permeability of a BSCF-based disk-shaped membrane with a porous BSCF layer deposited on the surface was studied in [44]. The oxygen flux was $J_{O_2} \sim 2.5$ mL/(min cm^2) at $T = 850$°C. In studying the oxygen permeation mechanism, the cited authors found that the oxygen transport process is governed by both bulk diffusion and surface exchange reactions, the contribution of which increases with an increase in temperature. In this case, the activation energies were 20 and 49 kJ/mol for the high-temperature and low-temperature regions, respectively.

It was shown [45] that the deposition of a porous layer of the $LaSr_{0.3}CoO_3$ (LSC) oxide on the surface of a BSCF disk-shaped membrane from the permeate side leads to an increase in the oxygen fluxes by a factor of 1.5–2. However, despite the surface modification, for all the BSCF membrane thicknesses (L = 0.5–1.5 mm), the oxygen permeability was limited to the mutual impact of the kinetics of surface reactions and solid-phase oxygen diffusion through the membrane.

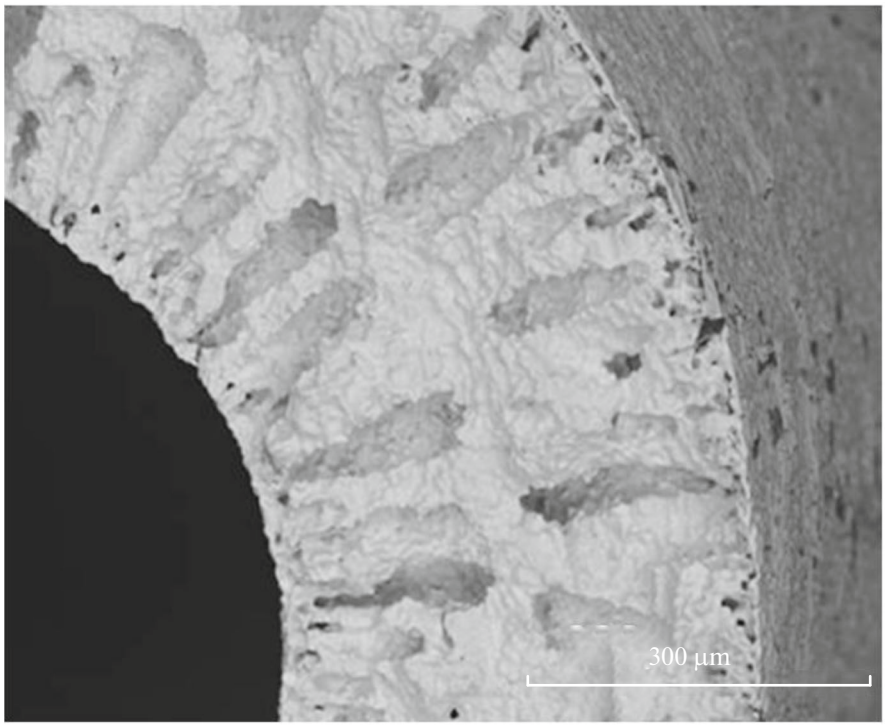

Fig. 3. Micrograph of an MT membrane based on the BSCFM10 oxide.

Data on an increase in oxygen permeability owing to the deposition of a coating of an ionic conductor based on ceria on the surface of a MOEC oxide membrane are provided in a number of studies [46–48]. The authors of [48] report that the deposition of a thin layer of a $Sm_xCe_{1-x}O_{2-\delta}$ (SDC) oxide on the surface of a $La_{0.6}Sr_{0.4}Co_{0.8}Fe_{0.2}O_{3-\delta}$ (LSCF) perovskite leads to an increase in the surface exchange rate by a factor of 10. This fact, in turn, suggests that, at the three-phase interface between the MOEC oxide, SDC, and the gaseous phase, oxygen exchange occurs quite readily. The cited authors showed that the exchange coefficient between LSCF and SDC increases with an increase in the ionic conductivity of the SDC. It is assumed that there is a synergistic effect between the compounds, which leads to an enhancement of the transport properties of the material [48].

MICROTUBULAR (MT) MEMBRANES BASED ON SCF AND BSCF

To date, the number of reports on the oxygen permeability of MT membranes, which are also referred to as hollow fibers, has significantly increased. In membranes of this type, a thin gas-tight layer with a thickness of 50–150 μm is localized between two porous layers; this factor, in turn, is responsible for the mechanical strength of the MT membrane (see Fig. 3). The developed surface of the porous layers and the small thickness of the gas-tight layer provide a significant increase in oxygen permeability. It is believed that MT membranes are the most demanded in the fields where the resistance of materials to various thermomechanical loads is required. In the field of oxygen separation and electricity generation using fuel elements, MT membranes have a higher specific power, mechanical strength, and resistance to thermal cycling; therefore, devices based on MT membranes can be rapidly started up.

Comparison of the oxygen permeabilities of disk-shaped and MT membranes based on the $Sr(Co_{0.8}Fe_{0.2})_{0.8}Ti_{0.2}O_{3-\delta}$ (SCFT20) oxide is described in [23]. According to the results of the studies, the oxygen flux of the MT membrane was higher than that of the SCFT20 disk-shaped membrane ($L = 1$ mm): $J_{O_2} \sim 1.92$ and 1.23 mL/(min cm^2), respectively. The activation energies for oxygen permeation were 58.2 ± 3.0 and 69.6 ± 10.1 kJ/mol for the MT and disk-shaped membranes, respectively. The cited authors showed that the oxygen transport process for disk-shaped and MT membranes based on the SCFT20 oxide is limited to the mutual impact of the kinetics of oxygen exchange on the surface and solid-phase oxygen diffusion. However, it should be noted that, in analyzing the oxygen transport, the cited authors did not take into account the specificity of oxygen permeability in MT membranes; therefore, these conclusions give rise to doubts.

The oxygen permeability of MT membranes based on the BSCF oxide was studied in [49]. The results of the study showed an increase in the oxygen fluxes by a

Table 2. Published data on the oxygen fluxes and activation energies for oxygen transport of MT membranes based on SCF/BSCF oxides

Composition	Conditions	Wall thickness, mm	$J(O_2)$, mL/(min cm^2)	E_a, kJ/mol
$Sr(Co_{0.8}Fe_{0.2})_{0.8}Ti_{0.2}O_{3-\delta}$ [23]	$T = 950°C$; $pO_{2.1} = 0.2$ atm	0.30	1.9	–
$SrCo_{0.8}Fe_{0.1}Ga_{0.1}O_{3-\delta}$ [74]	$T = 950°C$; $pO_{2.1} = 0.2$ atm	0.30	3.5	35–45
BSCF [50]	$T = 900°C$; $pO_{2.1} = 0.2$ atm	0.72	8.5	–
BSCF [51]	$T = 900°C$; $pO_{2.1} = 0.2$ atm	0.30	3.9	91
BSCF [43]	$T = 900°C$; $pO_{2.1} = 0.2$ atm	0.48	7.8	113
$BaCo_xFe_yZr_zO_{3-\delta}$ ($x + y + z = 1$) [56]	$T = 900°C$; $pO_{2.1} = 0.2$ atm	0.14	3.3	–
$Ba_{0.5}Sr_{0.5}Co_{0.8}Cu_{0.2}O_{3-\delta}$ (BSCC) [52]	$T = 900°C$; $pO_{2.1} = 0.2$ atm	0.17	5.8	–
$BaBi_{0.05}Sc_{0.1}Co_{0.85}O_{3-\delta}$ (BBSC) [51]	$T = 900°C$; $pO_{2.1} = 0.2$ atm	0.17	6.9	–
$Ba_{0.5}Sr_{0.5}Co_{0.78}W_{0.02}Fe_{0.2}O_{3-\delta}$ (BSCFW2) [54]	$T = 900°C$; $pO_{2.1} = 0.2$ atm	0.51	5.7	–
$BaBi_{0.05}Co_{0.8}Nb_{0.15}O_{3-\delta}$ (BBCN) [51]	$T = 900°C$; $pO_{2.1} = 0.2$ atm	0.45	7.1	–
$Bi_{0.05}Sc_{0.1}Co_{0.85}O_{3-\delta}$ [51]	$T = 920°C$; $pO_{2.1} = 0.2$ atm	0.17	9	127
$Ba_{0.5}Sr_{0.5}Co_{0.8}Fe_{0.175}Y_{0.025}O_{3-\delta}$ [55]	$T = 900°C$; $pO_{2.1} = 0.2$ atm	0.33	6.3	–
$Ba_{0.5}Sr_{0.5}Co_{0.75}Fe_{0.2}Mo_{0.05}O_{3-\delta}$ (BSCFM5) [43]	$T = 900°C$; $pO_{2.1} = 0.2$ atm	0.48	9.8	82

factor of 2.5 compared with the respective parameter of disk-shaped membranes based on BSCF. These results have aroused considerable interest in designing and modifying MT membranes based on the BSCF oxide. The oxygen permeability of MT membranes for compounds based on SCF/BSCF is shown in Table 2 [43, 50–52, 54–56].

It is known that the specific porous microstructure of MT membranes is formed due to the difference in the diffusion coefficients of the coagulant and the solvent in the phase inversion method [49, 50]. It was shown [49] that, by varying some characteristics, such as solution viscosity, extrusion rate, sintering temperature, and coagulant composition, in the phase inversion method, it is possible to significantly change the morphology of MT membranes and synthesize membranes with different arrangements of the gas-tight layer and porosity values.

The effect of the morphology of MT membranes on the oxygen permeability of the BSCF oxide was shown in [50].

The highest oxygen fluxes were obtained for a BSCF-based MT membrane, which had a gas-tight layer (200 μm) on the inner side of the membrane and a porous layer on the outer side ($T_{sint} = 1050°C$). The cited authors showed that the sintering of a BSCF-based MT membrane at $T > 1050°C$ leads to the disappearance of the specific porous structure and a decrease in the oxygen permeability. It should be noted that, in that study, the oxygen fluxes through the BSCF-based MT membrane remained stable at a level of $J_{O_2} \sim 8.5$ mL/(min cm^2) at $T = 900°C$ for 120 h.

The oxygen permeability of MT membranes based on the $BaBi_{0.05}Sc_{0.1}Co_{0.85}O_{3-\delta}$ (BBSC) perovskite, which had a gas-tight layer on the outer side and a porous layer on the inner side, was studied in [51]. The results of the study showed fairly high oxygen fluxes of $J_{O_2} \sim 11.4$ mL/(min cm^2) ($T = 950°C$; $F_{Ar} = 240$ mL/min). In determining the activation energy for the oxygen transport process, by plotting oxygen fluxes versus the reciprocal of temperature, a non-Arrhenius dependence of the curves was obtained. The activation energy was 127 kJ/mol at $T = 600–800°C$. However, an increase in T (°C) led to a decrease in the energy by 20–50% and the occurrence of a dependence on the carrier gas flow rate. According to the cited authors, the observed effects are associated with a change in the rate-limiting step of the oxygen permeation process and the dominant impact of the kinetics of oxygen exchange on the surface.

It was shown [52] that the substitution of iron cations by copper cations in the $Ba_{0.5}Sr_{0.5}Co_{1-x}Cu_xO_{3-\delta}$ (BSCC) oxide provides a high oxygen flux through an MT membrane at a level of $J_{O_2} \sim 27$ mL/(min cm^2) (at $T = 950°C$, $pO_{2.1} = 0.2$ atm, $F_{Ar} = 400$ mL/min). The cited authors attribute the obtained positive effect to the specific microstructure of the MT membrane based on BSCC (thin gas-tight layer inside the porous structure) and the catalytic properties of copper. However, the results of in situ X-ray diffraction analysis showed the presence of a hexagonal phase, which is known to lead to a decrease in oxygen fluxes and stability of membrane operation over time.

Figure 4 shows graphical comparison of oxygen fluxes of MT membranes based on BSCF oxides that

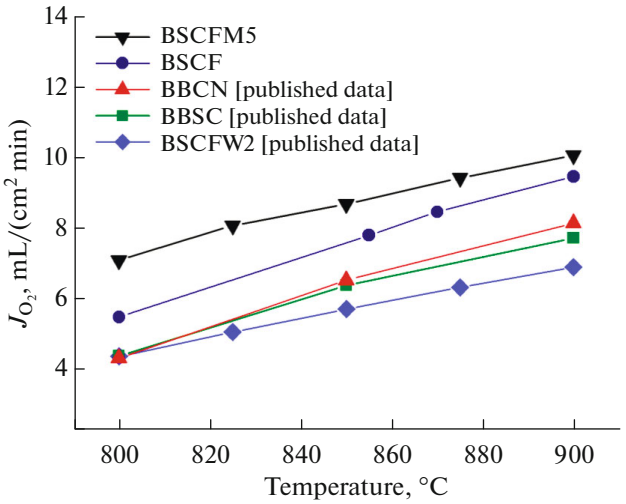

Fig. 4. Temperature dependence of the oxygen fluxes of MT membranes based on BSCF.

were synthesized under similar conditions. A record oxygen flux value for oxygen-permeable MT membranes was achieved using an MT membrane based on the $Ba_{0.5}Sr_{0.5}Co_{0.75}Fe_{0.2}Mo_{0.05}O_{3-\delta}$ (BSCFM5) oxide [43]. According to the results of the study, the high oxygen fluxes can be associated with the specific microstructure of the oxide, which consists of a self-assembled composite based on a cubic perovskite and a double perovskite.

It should be noted that, in comparing oxygen fluxes for MT membranes, many authors do not take into account the fact that membranes have different microstructures and, accordingly, different surface areas. In analyzing oxygen fluxes, these authors use the same formulas as those used for disk-shaped membranes. It was shown [53] that the oxygen flux varies along the length of the MT membrane, and the partial pressure of oxygen at the outlet $pO_{2.2}(L)$ is a nonlinear function of the length and diameter of the membrane and the carrier gas flow rate (see Fig. 5). Thus, to describe the oxygen transport through MT membranes and determine kinetic parameters that have a physical meaning, it is necessary to conduct a computer simulation of oxygen fluxes. The studies of the oxygen permeability of MT membranes using computer simulation showed that the oxygen transport in MT membranes based on $Ba_{0.5}Sr_{0.5}Co_{0.8-x}Fe_{0.2}Mo_xO_{3-\delta}$ (x = 0, 0.05) oxides is governed by exchange reactions on the surface [53].

MIXED OXYGEN–ELECTRONIC CONDUCTIVITY OXIDES AS ELECTRODES FOR SOFCs

A global contemporary issue is the energy problem, which implies not only the depletion of nonrenewable energy resources, but also environmental pollution caused by emissions from fuel combustion, the amount of which is growing every year. Currently, the issue of alternative energy is relevant from both an environmental and economic point of view. One of the most promising solutions is the development of fuel cells in which a hydrocarbon fuel and/or hydrogen undergoes an efficient transformation (efficiency of about 60–80%) directly into electricity [57, 58].

Currently, SOFCs are the most promising type. The main advantages of SOFCs are the high process efficiency and the possibility of using various types of fuel (natural gas, biogas, etc.). In a SOFC, a thin gas-tight electrolyte layer is localized between porous electrodes; at the cathode, molecular oxygen from air is reduced to oxide ions by electrons from the external circuit. Oxygen ions diffuse through the electrolyte layer to the anode, where they are oxidized while interacting with the fuel. In the process, electrons are formed; they flow into the external circuit and, via a load, arrive at the cathode (see Fig. 6).

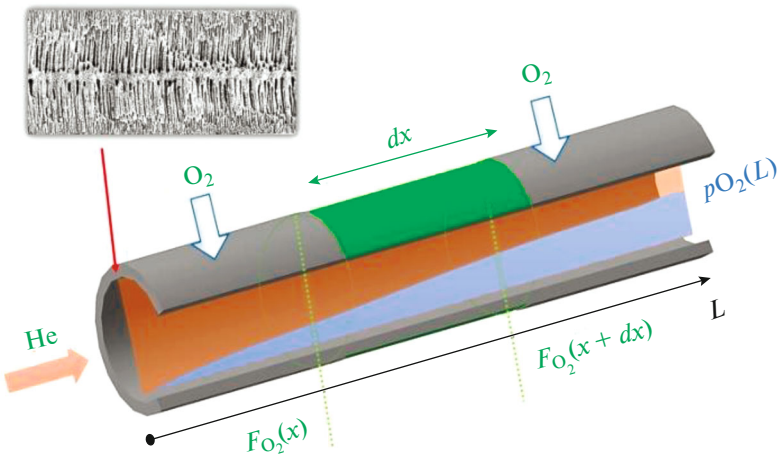

Fig. 5. Graphical representation of the distribution of oxygen fluxes through an MT membrane.

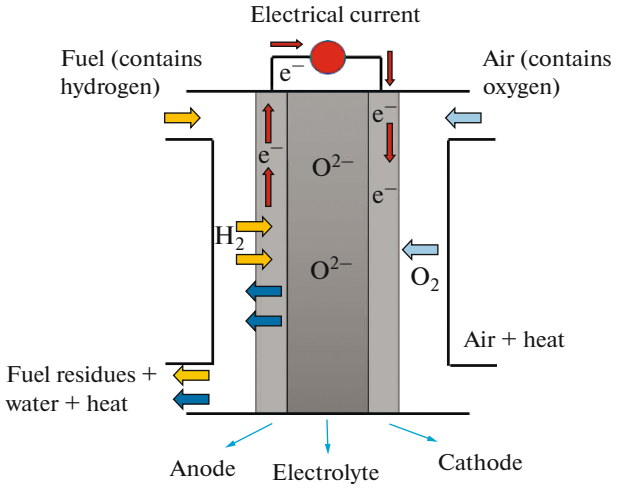

Fig. 6. Schematic diagram of the operation principle of SOFCs.

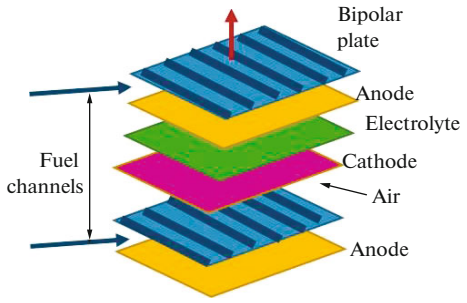

Fig. 7. Schematic diagram of a planar SOFC.

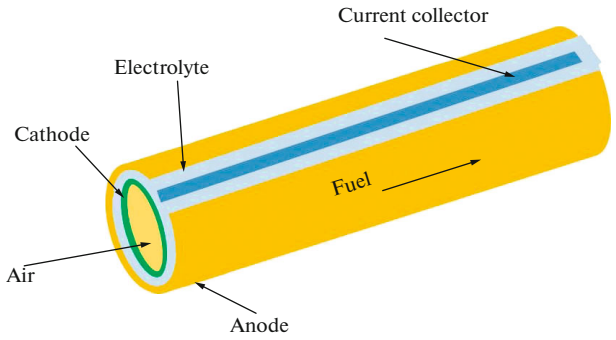

Fig. 8. Schematic diagram of a tubular SOFC.

The SOFC designs are as follows: planar, segmental, tubular, block, monolithic, etc. [58]. Planar SOFCs (see Fig. 7) are used for high-power energy generation. However, this type is characterized by structural losses, which impose additional requirements for electrode materials (decreasing the thickness and resistance of the electrode, increasing the electronic conductivity, etc.) [59]. Tubular SOFCs (see Fig. 8) are most commonly used to design mobile and portable electric power generators, various gadgets, and military devices, where the important parameters are actuation speed and resistance to temperature changes and electrical loads [59].

It is known that the SOFC temperature varies in a range of 600–1000°C; this factor, in turn, makes it possible to use of various types of fuel without subjecting them to a special treatment. However, high temperatures necessitate the use of appropriate electrode and electrolyte materials exhibiting structural stability and high electrochemical characteristics. It is known that, with a decrease in the SOFC temperature, the operating efficiency significantly decreases due to the polarization resistance of the electrode materials. To date, the problem of designing medium-temperature SOFCs has not been solved; it requires the search for new cathode materials exhibiting high electrochemical characteristics and chemical and thermomechanical stability [58, 60].

ELECTRODE MATERIALS FOR SOFCs

Conventional cathode materials in SOFCs are $La_{1-x}Sr_xMnO_{3-\delta}$ and $La_{1-x}Sr_xFe_{1-y}Co_yO_{3-\delta}$ perovskites; their significant disadvantage is interaction with the electrolyte material (yttria-stabilized zirconia (YSZ) and gadolinium-doped ceria (GDC)) to form impurity phases that hinder oxygen transport [61, 62]. Table 3 lists the electrochemical characteristics of electrode materials based on MOEC oxides. According to [24, 63–65], one of the most promising cathode materials for SOFCs is the BSCF oxide. It was shown [65] that, for the BSCF oxide, the peak power densities were 1010 and 402 mW cm^{-2} at $T = 600$ and 500°C, respectively. However, the BSCF oxide has a fairly high coefficient of thermal expansion (CTE) with a value of more than 20×10^{-6} K^{-1} at $T = 50$–1000°C [65]. In addition, as noted earlier, this compound is characterized by structural instability in a CO_2 atmosphere, which leads to an increase in the polarization and ohmic resistance of the cathode material.

The authors of [13, 64] attribute the high CTE values of BSCF to the high cobalt content in the structure. However, the authors of [66] argue against this assumption; they show that a decrease in the cobalt content due to an increase in the iron content does not lead to an improvement of the electrochemical characteristics of the material. The results of the study showed that an increase in the iron content in the BSCF structure leads to an increase in the resistivity and a decrease in the electrical conductivity.

One of the known methods to control the electrochemical properties of cathode materials based on the BSCF oxide is the surface modification of the electrode. The authors of [67] showed improved cathodic characteristics of a BSCF-based oxide with a $Ce_{0.8}Sm_{0.2}O_{1.9}$ (SDC) layer on the surface in a tubular SOFC. The cell performance was significantly improved; in the case of using hydrogen as the fuel, the

Table 3. Published data on the electrochemical characteristics of electrodes based on MOEC oxides

Electrode composition	Electrolyte composition	Temperature	Conditions (fuel)	Peak power density, mW cm^{-2}	Resistivity, Ω cm^2
$La_{0.5}Sr_{0.5}Co_{0.8}Fe_{0.2}O_{3-\delta}$ cathode [62]	GDC	650°C	H_2	562	0.27
$Ba_{0.5}Sr_{0.5}Co_{0.8}Fe_{0.2}O_{3-\delta}$ cathode [65]	$Ce_{0.8}Sm_{0.2}O_{1.9}$ (SCD)	500°C	H_2	402	0.23
$Ba_{0.5}Sr_{0.5}Co_{0.8}Fe_{0.2}O_{3-\delta}$ – SDC cathode [67]	SDC	560°C	H_2	640	0.43
$Ba_{0.5}Sr_{0.5}Co_{0.8}Fe_{0.2}O_{3-\delta}$ CoO_x cathode [66]	SDC	500°C	H_2 (3%H_2O)	463	1.1
$Ba_{0.5}Sr_{0.5}Co_{0.8}Fe_{0.2}O_{3-\delta}$ GDC cathode [68]	$Gd_{0.1}Ce_{0.9}O_{1.9}$ (GDC)	500°C	H_2 (3%H_2O)	447	–
$Ba_{0.5}Sr_{0.5}Co_{0.8}Fe_{0.2}O_{3-\delta}$–$LaCoO_{3-\delta}$ (LC) cathode [68]	GDC	600°C	H_2 (3%H_2O)	588	1.17
$Ba_{0.5}Sr_{0.5}Co_{0.75}Nb_{0.05}O_{3-\delta}$ cathode [69]	SDC	700°C	H_2 (3%H_2O)	882	0.14
$Ba_{0.5}Sr_{0.5}Co_{0.7}Fe_{0.2}Mo_{0.1}O_{3-\delta}$ cathode/anode [70]	GDC/YSZ	700°C	H_2 (3%H_2O)	268	0.71
$Ba_{0.5}Sr_{0.5}Co_{0.8}Fe_{0.2}O_{3-\delta}$ cathode/anode [70]	GDC/YSZ	700°C	H_2 (3%H_2O)	139	1.38
$Ba_{0.5}Sr_{0.5}(Co_{0.7}Fe_{0.3})_{0.6875}W_{0.3125}O_{3-\delta}$ [42]	–	650°C	H_2	–	0.034
$Nd_{0.2}Sr_{0.8}Nb_{0.1}Co_{0.9}O_{3-\delta}$ ($N_{0.2}$SNC) cathode [71]	SDC	650°C	H_2	1563	0.141

peak power density achieved a value of 495 mW cm^{-2} (T = 700°C). It was shown [68] that the electrochemical characteristics of a cathode material based on BSCF significantly deteriorate in the presence of a metal current collector containing Cr_2O_3. The cited authors showed that a $LaCoO_{3-\delta}$ (LC) coating on a BSCF cathode can improve both the electrochemical characteristics and structural stability of the cathode material under operating conditions. The results of electrochemical studies of a fuel cell with an LC–BSCF cathode and a $Gd_{0.1}Ce_{0.9}O_{1.9}$ (GDC) electrolyte showed a significant increase in the peak power density (Table 3) and a decrease in the polarization resistance compared with the respective parameters of the BSCF–GDC cathode. In addition, for single cells with an LC–BSCF cathode and a GDC electrolyte, a significant improvement in the stability of operation at a constant current load was achieved.

The authors of [66] modified the surface of the BSCF oxide by depositing a CoO_x oxide layer exhibiting catalytic activity. According to the results of electrochemical studies, the electrical conductivity of the cathode material was significantly increased, while the peak power density was 463 mW cm^{-2} at T = 500°C.

According to [42, 43, 69], the introduction of highly charged cations (Nb, W, Mo) into BSCF is a promising method to synthesize cathode materials with improved electrochemical characteristics. For example, the authors of [42] showed that the total area specific resistance (ASR) of a cathode material based on the $Ba_{0.5}Sr_{0.5}(Co_{0.7}Fe_{0.3})_{0.6875}W_{0.3125}O_{3-\delta}$ (BSCFW) oxide was 0.034 Ω cm^2 at T = 650°C at the beginning of the experiment and 0.039 Ω cm^2 after 60 h. It should be noted that the obtained values are several times lower than those of conventional cathode materials.

The authors of [69] studied $Ba_{0.5}Sr_{0.5}Co_{0.8-x}Fe_{0.2}Nb_xO_{3-\delta}$ ($x \le 0.1$) (BSCFNb$_x$) oxides as potential cathode materials. The results of the study showed that, with an increase in the niobium content in the BSCF structure, the structural stability in a CO_2 atmosphere increases, while the electrical conductivity of the oxide decreases. The authors report that the $Ba_{0.5}Sr_{0.5}Co_{0.75}Fe_{0.2}Nb_{0.05}O_{3-\delta}$ (BSCFNb$_{0.05}$) oxide has the highest electrochemical characteristics (peak power density of 882 mW cm^{-2}) and the lowest resistivity of 0.14 Ω cm^2 at T = 700°C. The fuel cell with a BSCFNb0.05 cathode maintains a specific power of 400 mW cm^{-2} for 70 h; this fact suggests that this oxide is a promising cathode material for SOFCs.

Oxides based on $Ba_{0.5}Sr_{0.5}Co_{0.8-x}Fe_{0.2}Mo_xO_{3-\delta}$ ($0 \le x \le 0.1$) (BSCFM$_x$) were studied as potential cathode materials in [43]. It was shown that doping with molybdenum cations leads to an increase in the total conductivity, which is associated with the microstructural features of the synthesized materials. Using in situ and ex situ X-ray diffraction, it was shown that materials based on $Ba_{0.5}Sr_{0.5}Co_{0.7}Fe_{0.2}Mo_{0.1}O_{3-\delta}$ (BSCFM10) exhibit a fairly high chemical compatibility with an electrolyte based on $Ce_{0.8}Gd_{0.2}O_{3-\delta}$ (CGO), which is used in medium-temperature SOFCs. Of interest are the electrochemical data of cathode materials described in [70]. The results of the studies showed that an electrode material based on $Ba_{0.5}Sr_{0.5}Co_{0.2}Fe_{0.7}Mo_{0.1}O_{3-\delta}$ exhibits a fairly high stability in reducing and oxidizing atmospheres and has improved electrochemical parameters. Upon the intro-

duction of molybdenum cations (10%) into the BSCF structure, a decrease in the polarization resistance is observed, while the peak power density achieves a value of 418 mW cm^{-2} (in the case of using wet H_2) at T = 800°C. A BSCF/GDC/YSZ/GDC/BSCFM fuel cell (where GDC is a buffer layer, YSZ is an electrolyte) exhibited a stable operation at T = 700°C for 115 h. The cited authors report that the efficiency of BSCFM is significantly higher than that of BSCF due to the catalytic activity of the BSCFM oxide.

The implementation and widespread use of the SOFC technology require cathode materials exhibiting high electrochemical activity and long-term stability at low temperatures in a CO_2 atmosphere. The authors of [71] report on a new $Nd_{0.2}Sr_{0.8}Nb_{0.1}Co_{0.9}O_{3-\delta}$ ($N_{0.2}$SNC) perovskite-like oxide synthesized by codoping with Nd^{3+} and Nb^{5+} cations in the A- and B-sites of the perovskite structure, respectively. The results of X-ray diffraction analysis of the $N_{0.2}$SNC oxide exposed to a CO_2 atmosphere for 20 h did not show the presence of additional phases; this fact suggests that the material exhibits chemical stability under the above conditions. Studies of the power characteristics of the fuel cell showed that, in the case of using the $N_{0.2}$SNC oxide as a cathode material, the peak power density was 1563 mW cm^{-2} at T = 650°C, which is a record value for the known cathode materials. The cited authors report that a significant increase in the electrochemical characteristics and chemical stability was achieved due to the synergistic effect between the A and B cations. Thus, the isomorphic substitution of A and B cations of MOEC oxides is an effective strategy for improving both the chemical stability and electrochemical characteristics of cathode materials.

CONCLUSIONS

According to the published data, the SCF perovskite is a promising material for various technological processes, because it has high transport characteristics. However, SCF-based materials are characterized by a low phase stability in a CO_2 atmosphere and at low oxygen partial pressures. This feature, in turn, has an adverse effect on the oxygen permeability and leads to a significant degradation of the material. To improve the phase stability and transport characteristics of SCF-based materials, doping with cations with a stable oxidation state (Al^{3+}, Zr^{4+}, Ti^{4+}) in the B-site of the perovskite structure is commonly used. However, this doping is accompanied by a significant decrease in the oxygen permeability. The highest oxygen fluxes for conventional membrane materials based on MOEC perovskites are observed for the BSCF oxide and derivatives of this oxide. However, the structure of the BSCF oxide is characterized by a low chemical stability in a CO_2 atmosphere and the occurrence of phase transformations at $T \le 850$°C to form various polymorphic species, which is accompanied by a decrease in the transport characteristics. The initiation of a composite disorder in the structure of SCF and BSCF oxides using isomorphic substitution with ferroactive highly charged cations with a stable oxidation state (Nb, Ta, Mo, W) can significantly improve both the phase/chemical stability and transport characteristics of the materials.

Currently, MT membranes are being intensively developed and studied, because they are most promising for industrial applications in various technologies. According to the published data, the oxygen permeability of MT membranes based on the BSCF oxide is extremely high. However, many authors compare the oxygen fluxes of BSCF-based MT membranes without taking into account the microstructural features. According to recent studies, to describe the oxygen transport across MT membranes and determine kinetic parameters that have a physical meaning, it is necessary to conduct a computer simulation of oxygen fluxes taking into account the membrane geometry.

In the field of designing SOFCs, the most urgent task is to search for new cathode materials exhibiting low resistivity and polarizability (i.e., high oxygen exchange rates). Currently, a promising cathode material is BSCF-based oxides. To provide their effective use, it is necessary to improve their electrochemical characteristics, while maintaining chemical and structural stability; this problem can be solved by introducing highly charged cations and modifying the electrode surface.

FUNDING

This work was performed under a state task to Institute of Solid State Chemistry and Mechanochemistry of the Siberian Branch of the Russian Academy of Sciences (project nos. 121032500059-4 and FWUS-2021-0001).

REFERENCES

1. J. B. Goodenough, Rep. Progr. Phys. **67**, 1915 (2004).
2. Yu. I. Smolikov, Yu. F. Shepelev, and A. A. Levin, Zh. Neorg. Khim. **34**, 2451 (1989).
3. J. B. Yang, J. Kim, Y. S. Woo, C. S. Kim, and B. W. Lee, J. Magn. Magn. Mater. **310**, 664 (2007).
4. G. Burns and F. Dacol, Solid State Commun. **48**, 853 (1983).
5. V. V. Kharton, M. V. Patrakeev, J. C. Waerenborgh, V. A. Sobyanin, S. A. Veniaminov, A. A. Yaremchenko, P. Gaczynski, V. D. Belyaev, G. L. Semin, and J. R. Frade, Solid State Sci. **7**, 1344 (2005).
6. S. Sharma, M. Tomar, A. Kumar, N. K. Puri, and V. Gupta, J. Phys. Chem. **93**, 63 (2016).
7. J. Zhang, X. Gao, Y. Deng, Y. Zha, and C. Yuan, Solar Energy Mater. Solar Cells **166**, 9 (2017).
8. A. Vassilakopoulou, D. Papadatos, and I. Koutselas, Microporous Mesoporous Mater. **249**, 165 (2017).

9. H. J. M. Bouwmeester and A. J. Burggraf, in *The CRC Handbook of Solid State Electrochemistry,* Ed. by P. J. Gellings and H. J. M. Bouwmeester (CRC Press, 1997).
10. M. Tang, L. Xu, and M. Fan, Appl. Energy **151**, 143 (2015).
11. Y. Teraoka, H. Zhang, S. Furukawa, and N. Yamazoe, Chem. Lett. **14**, 1743 (1985).
12. S. Li, Z. Tang, F. Zhou, W. Li, and X. Yuan, Chinese J. Chem. Eng. **22**, 980 (2014).
13. J. Sunarso, S. S. Hashim, N. Zhu, and W. Zhou, Progr. Energy Combust. Sci. **61**, 57 (2017).
14. Z. Shao, G. Xiong, J. Tong, H. Dong, and W. Yang, Sep. Purif. Technol. **25**, 419 (2001).
15. Z. Shao, W. Yang, Y. Cong, H. Dong, J. Tong, and G. Xiong, J. Membr. Sci. **172**, 177 (2000).
16. H. Lu, J. P. Kim, S. H. Son, and J. H. Park, Mater. Lett. **65**, 2858 (2011).
17. I. A. Starkov, S. F. Bychkov, S. A. Matvienko, and A. P. Nemudry, Phys. Chem. Chem. Phys. **16**, 5527 (2014).
18. A. P. Nemudry, J. Membr. Sci. **539**, 313 (2017).
19. X. Dong, Z. Liu, Y. He, W. Jin, and N. Xu, J. Membr. Sci. **331**, 109 (2009).
20. W. Chen, Y. B. Zuo, C. S. Chen, and A. J. A. Winnubst, Solid State Ionics **181**, 971 (2010).
21. W. Chen, C. Chen, and L. Winnubst, Solid State Ionics **196**, 30 (2011).
22. Y. Liu, S. Baumann, F. Schulze-Küppers, D. Mueller, and O. Guillon, J. Eur. Ceram. Soc. **38**, 5058 (2018).
23. J. Li, Q. Zeng, T. Liu, and C. Chen, Sep. Purif. Technol. **77**, 76 (2011).
24. M. P. Popov, I. A. Starkov, S. F. Bychkov, and A. P. Nemudry, J. Membr. Sci. **469**, 88 (2014).
25. M. P. Popov, S. F. Bychkov, and A. P. Nemudry, Dokl. Phys. Chem. **465**, 263 (2015).
26. F. Vente, S. McIntosh, W. G. Haije, and H. J. M. Bouwmeester, J. Solid State Electrochem. **10**, 581 (2006).
27. K. Efimov, Q. Xu, and A. Feldhoff, Chem. Mater. **22**, 5866 (2010).
28. M. Meffert, L. Unger, H. Stormer, F. Sigloch, S. Wagner, E. Ivers-Tiffee, and D. Gerthsen, J. Am. Ceram. Soc. **102**, 4929 (2019).
29. M. Arnold, H. Wang, and A. Feldhoff, J. Membr. Sci. **293**, 44 (2007).
30. D. Matras, A. Vamvakeros, S. D. M. Jacques, V. Middelkoop, G. Vaughan, M. A. Aran, R. J. Cernika, and A. M. Beale, Phys. Chem. Chem. Phys. **22**, 18964 (2020).
31. X. Zhang, J. Motuzas, S. Liu, and J. C. Diniz da Costa, Sep. Purif. Technol. **189**, 399 (2017).
32. P. Haworth, S. Smart, J. Glasscock, and J. C. Diniz da Costa, Sep. Purif. Technol. **94**, 16 (2012).
33. O. Ravkina, T. Klande, and A. Feldhoff, J. Solid State Chem. **201**, 101 (2013).
34. Z. R. Ismagilov, V. V. Kriventsov, D. I. Kochubey, Z. R. Ismagilov, O. Yu. Podyacheva, and A. P. Nemudry, Phys. Scr. **115**, 740 (2005).
35. I. L. Zhogin, A. P. Nemudry, P. V. Glyanenko, Y. M. Kamenetsky, H. J. M. Bouwmeester, and Z. R. Ismagilov, Catal. Today **118**, 151 (2006).
36. O. A. Savinskaya and A. P. Nemudry, and N. Z. Lyakhov, Inorg. Mater. **43**, 1350 (2007).
37. I. V. Belenkaya, A. A. Matvienko, and A. P. Nemudry, J. Mater. Chem. A **46**, 23240 (2015).
38. I. Belenkaya, A. Matvienko, and A. Nemudry, J. Appl. Crystallogr. **48**, 179 (2015).
39. O. A. Savinskaya and A. P. Nemudry, J. Membr. Sci. **459**, 45 (2014).
40. A. P. Nemudry, J. Membr. Sci. **539**, 313 (2017).
41. A. Demont, R. Sayers, M. A. Tsiamtsouri, S. Romani, P. A. Chater, H. Niu, C. Marti-Gastaldo, Z. Xu, Z. Deng, Y. Bréard, M. F. Thomas, J. B. Claridge, and M. J. Rosseinsky, J. Am. Chem. Soc. **135**, 10114 (2013).
42. F. Shin, W. Xu, M. Zanella, K. Dawson, S. N. Savvin, J. B. Claridge, and M. J. Rosseinsky, Nature Energy **2**, 1624 (2017).
43. E. V. Shubnikova, O. Bragina, and A. P. Nemudry, J. Ind. Eng. Chem. **59**, 242 (2017).
44. K. Ishii, C. Matsunaga, K. Kobayashi, A. J. Stevenson, C. Tardivat, and T. Uchikoshi, J. Eur. Ceram. Soc. **39**, 5292 (2019).
45. W. K. Hong and G. M. Choi, J. Membr. Sci. **346**, 353 (2010).
46. J. Richter, P. Holtappels, T. Graule, T. Nakamura, and L. J. Gauckler, Monatsh. Chem. Chem. Mon. **140**, 985 (2009).
47. B. He, D. Ding, Y. Ling, J. Xu, and L. Zhao, J. Membr. Sci. **477**, 7 (2015).
48. T. Hong, L. Zhang, F. Chen, and C. Xia, J. Power Sources **218**, 254 (2012).
49. S. Liu and G. R. Gavalas, J. Membr. Sci. **246**, 103 (2005).
50. D. Han, X. Tan, Z. Yan, Q. Li, and S. Liu, Ceram. Int. **39**, 431 (2013).
51. Z. Wang, Y. Kathiraser, T. Soh, and S. Kawi, J. Membr. Sci. **465**, 151 (2014).
52. A. Leo, J. Motuzas, C. Yacou, S. Liu, J. M. Serra, L. Navarrete, J. Drennan, A. Julbe, and J. C. Diniz da Costa, J. Membr. Sci. **526**, 323 (2017).
53. M. P. Popov, S. F. Bychkov, S. A. Chizhik, and A. P. Nemudry, Chem. Eng. J. **372**, 251 (2019).
54. S. F. Bychkov and A. P. Nemudry, Solid State Ionics **312**, 73 (2017).
55. P. Haworth, S. Smart, and J. Glasscock, and J. C. Diniz da Costa, Sep. Purif. Technol. **94**, 16 (2012).
56. O. Czuprat, M. Arnold, S. Schirrmeister, T. Schiestel, and J. Caro, J. Membr. Sci. **364**, 132 (2010).
57. M. Irshad, K. Siraj, R. Raza, A. Ali, P. Tiwari, B. Zhu, A. Rafique, A. Ali, M. K. Ullah, and A. Usman, Appl. Sci. **6**, 75 (2016).
58. S. P. Filippov and A. B. Yaroslavtsev, Russ. Chem. Rev. **90**, 627 (2021).
59. A. S. Lipilin, Elektrokhim. Energ. **7**, 61 (2007).
60. S. M. Jamil, M. H. D. Othman, M. A. Rahman, J. Jaafar, A. F. Ismail, and K. Li, J. Eur. Ceram. Soc. **35**, 1 (2015).
61. Y. He, L. Fan, M. Afzal, M. Singh, W. Zhang, Y. Zhao, J. Li, and B. Zhu, Electrochim. Acta **191**, 223 (2016).
62. S. Ya. Istomin, N. V. Lyskov, G. N. Mazo, and E. V. Antipov, Russ. Chem. Rev. **90**, 644 (2021).

63. A. A. Yaremchenko, M. V. Patrakeev, E. N. Naumovich, and D. D. Khalyavin, Phys. Chem. Chem. Phys. **20**, 4442 (2018).

64. S. M. Fang, C. Y. Yoo, and H. J. M. Bouwmeester, Solid State Ionics **195**, 1 (2011).

65. Z. P. Shao and S. M. Haile, Nature **431**, 170 (2004).

66. Y. He, L. Fan, M. Afzal, M. Singh, W. Zhang, Y. Zhao, J. Li, and B. Zhu, Electrochim. Acta **191**, 223 (2016).

67. M. Afzal, S. Madaan, W. Dong, R. Raza, C. Xia, and B. Zhu, Int. J. Hydrogen Energy **42**, 17536 (2017).

68. P. Qiu, J. Li, L. Jia, B. Chi, J. Pu, J. Li, and F. Chen, Electrochim. Acta **319**, 981 (2019).

69. Y. Huang, J. Ding, Y. Xia, L. Miao, K. Li, Q. Zhang, and W. Liu, Ceram. Int. **46**, 10215 (2020).

70. X. Yang, R. Li, Y. Yang, G. Wen, D. Tian, X. Lu, Y. Ding, Y. Chen, and B. Lin, J. Alloys Compd. **831**, 154711 (2020).

71. J. Zhang, X. Li, Z. Zhang, X. Xu, Y. Chen, Y. Song, J. Dai, G. Yang, R. Ran, W. Zhou, and Z. Shao, J. Power Sources **457**, 227995 (2020).

Translated by M. Timoshinina